Use One-bit Technique to Measure the Coherence in the Time, Frequency and Space Domain in a Reverberation Chamber

Qian Xu[1*], Lei Xing[1], Yongjiu Zhao[1], Tianyuan Jia[2] and Yi Huang[2]

[1] College of Electronic and Information Engineering, Nanjing University of Aeronautics and Astronautics, Nanjing, China
[2] Department of Electrical Engineering and Electronics, University of Liverpool, Liverpool, United Kingdom.
[*]emxu@foxmail.com

Abstract: High speed data streams are everywhere in the fifth generation (5G) system measurement. To develop a high efficient and low cost 5G testbed in a reverberation chamber, we propose a high efficient measurement method in the time, frequency and space coherence measurement. In this paper, the one-bit technique is introduced to measure the time domain, frequency domain and space domain correlations in a reverberation chamber. The coherence time, the coherence bandwidth and the correlated angle can all be measured using the one-bit correlation; float number calculations are simplified to logical operations which accelerate the data processing greatly. Measurements are performed to verify the results.

1. Introduction

A reverberation chamber (RC) is a highly resonant electrically large cavity and the statistical behaviour of the propagation channel inside an RC can be controlled using various strategies [1-4]. An RC provides a controllable statistical environment for the over-the-air (OTA) test in the fifth generation (5G) system measurements [5-13]. While general instruments can support most measurements, specifically tailored or programmable instruments such as universal software radio peripheral (USRP) or field-programmable gate array (FPGA) could be highly efficient and low cost for specific tasks [9, 14-17]. Since the 5G data stream is much faster than that in previous systems, a high efficient testbed for the OTA measurements in an RC is necessary.

In this paper, we introduce the one-bit technique (which only records the signs of the signal) into the OTA measurements. It could be highly efficient for some measurements especially for programmable hardware devices. One-bit technique has been used in high-resolution Earth tomography [18], real-time ultrasonic distance measurement [19], acoustic wave imaging [20], and pattern recognition [21]. In an RC, the one-bit technique has been applied to time reversal wave focusing [22]. Because of the simplicity and the high efficiency, the calculation cost for the correlation can be reduced greatly. In the meanwhile, the one-bit correlation can actually produce better results [23] when the interference level is high. It has been generalised in [24] that, even for nonstationary process, the one-bit correlation technique can still be applied.

If we check the statistical behaviour of an electromagnetic reverberation chamber (RC), the real/imaginary part of the frequency domain (FD) response has a Gaussian distribution [1] and the time domain (TD) response is a nonstationary process with Gaussian distribution [25]. They both satisfy the mathematical preconditions of one-bit correlation technique in [23]. In RC OTA measurements, the time/frequency/angular correlations are important parameters in TD channel emulation, Q factor measurement, and independent sample estimation, respectively. We expect these parameters can be obtained in measurements (real time) without using specific instruments. Since the original time/frequency/angular correlations can be reverted from the one-bit correlation, we can apply the one-bit correlation technique in RC measurements to accelerate the data processing and simplify the calculations.

This paper focuses on the time, frequency and space domain correlation measurements in an RC. Section 2 introduces the definition of one-bit correlation, Section 3 validates the results with measurements, discussion and conclusions are finally drawn in Section 4.

2. One-bit Correlation Definition

For a time dependent random variable $s(t)$, the autocorrelation function is defined as [6, 7, 24, 26-28]

$$R(\partial t) \equiv \frac{1}{T}\int_0^T s(t)s^*(t+\partial t)dt \qquad (1)$$

where ∂t is the variable for the coherence time, * means complex conjugate (if $s(t)$ is a complex signal), T is the duration for the integral. The autocorrelation can be defined in the FD by replacing $s(t)$ and ∂t with $S(f)$ and ∂f respectively,

$$R(\partial f) \equiv \frac{1}{f_2 - f_1}\int_{f_1}^{f_2} S(f)S^*(f+\partial f)df \qquad (2)$$

In this case, $S(f)$ is the FD response, ∂f is the variable for the frequency lag [6, 7, 26-29], f_1 and f_2 are the start and the stop frequencies for the integral respectively. Similarly, $s(t)$ and ∂t can also be replaced by using $S(\theta)$ and $\partial\theta$ in the space domain (SD) to characterise the angular correlation [28, 30]

$$R(\partial\theta) \equiv \frac{1}{\theta_2 - \theta_1}\int_{\theta_1}^{\theta_2} S(\theta)S^*(\theta + \partial\theta)d\theta \qquad (3)$$

where $S(\theta)$ is the FD response and depends on the rotation angle (θ) of a stirrer in an RC, $\partial\theta$ is the variable for the correlated angle, θ_1 and θ_2 represents the start and the stop rotation angle for the integral respectively.

If $s(t)$ is real, the one-bit form of $s(t)$ can be obtained by applying the binary filter [18-24]

$$s_b(t) = \begin{cases} 1 & \text{if } s(t) \geq 0 \\ -1 & \text{if } s(t) < 0 \end{cases} \qquad (4)$$

If $s_1(t)$ and $s_2(t)$ are two TD signals, the one-bit correlation is defined as

$$R_{b12}(\partial t) = \frac{1}{T}\int_0^T s_{b1}(t)s_{b2}(t + \partial t)dt \qquad (5)$$

where $s_{b1}(t)$ and $s_{b2}(t)$ are the one-bit versions of $s_1(t)$ and $s_2(t)$ respectively. It has been proven that the original correlation (correlation from the original signal) and the one-bit correlation $R_{b12}(\partial t)$ have a relationship of [24]

$$\langle R_{12}\rangle(\partial t) = \sigma_1\sigma_2 \sin\left[\frac{\pi}{2}\langle R_{b12}\rangle(\partial t)\right] \qquad (6)$$

where $\sigma_i^2 = \langle s_i^2(t)\rangle$, i=1, 2, and $\langle\cdot\rangle$ means the ensemble average for different stirrer positions. Specifically, for the autocorrelation when $s_{b1}(t) = s_{b2}(t) = s_b(t)$, the normalised correlation can be obtained from (6) as [23, 24, 31, 32]

$$\langle R\rangle_{norm}(\partial t) = \sin\left[\frac{\pi}{2}\langle R_b\rangle_{norm}(\partial t)\right] \qquad (7)$$

where the subscript *norm* means the normalised correlation. It is interesting to note that the information of the original correlation still holds even when the sign of the signal is recorded, thus we can use the one-bit correlation to recover the original correlations in an RC.

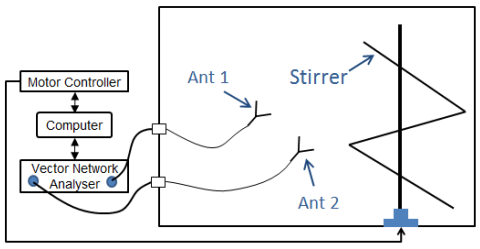

a

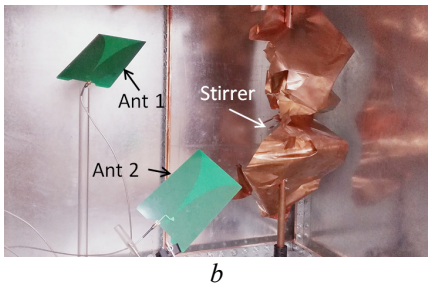

b

Fig. 1. **(a)** schematic plot , **(b)** measurement scenario.

3. Measurements

The schematic plot of the measurement setup is illustrated in Fig.1*a*, Ant 1 and Ant 2 are broadband Vivaldi antennas which connect to the Port 1 and Port 2 of a vector network analyser (VNA), respectively. The topology of the antenna is similar to that in [33], and the antennas are well-matched in the frequency range of 850 MHz – 6 GHz ($S_{11} < -10$ dB). Fig.1*b* gives the practical measurement scenario, and the dimensions of the RC are 0.8 m (width) × 1.2 m (length) × 1.2 m (height). The diameter of the stirrer is 40 cm and the height is 1 m. The lowest usable frequency is about 1 GHz [4].

3.1. Time Domain

The TD response can be obtained from the FD response by applying the inverse Fourier transform (IFT) to the measured S_{21} [25, 26, 28]. To demonstrate this process, we measured the S_{21} in the frequency range of 1 GHz ~ 3 GHz, 20001 frequency sample points were used. The measurement was repeated for 360 stirrer positions (1°/step).

A typical set of measured S_{21} at one stirrer position is given in Fig. 2*a*, the IFT of which is illustrated in Fig.2*b*. By filtering the TD response in Fig.2*b* using (4), a zoom-in view of the one-bit TD response is shown in Fig.2*c*. The normalised autocorrelations calculated using (1) and (7) are presented in Fig.3, as expected, they agree with each other very well.

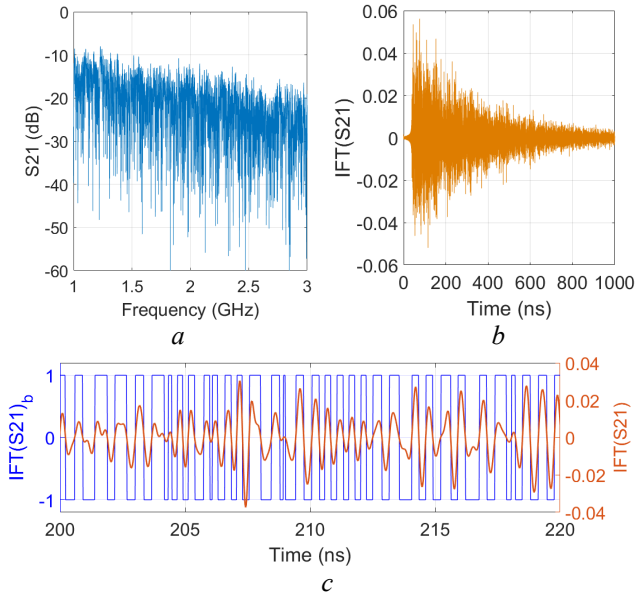

Fig.2. **(a)** Measured S_{21} at one stirrer position, **(b)** the IFT of the measured S_{21}, **(c)** the one-bit form of (b) after applying (4), only 200 ns - 220 ns is given to have a zoom-in view; IFT(S_{21}) means the IFT of the measured S_{21}, IFT$(S_{21})_b$ means the binary form of IFT(S_{21}).

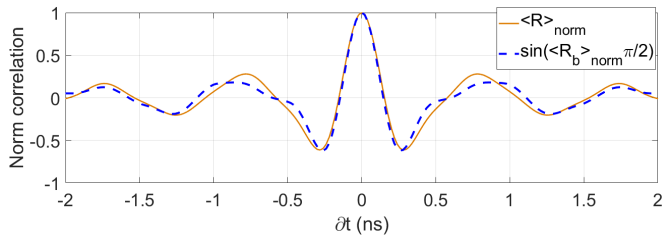

Fig.3. Normalised autocorrelations calculated from float numbers ($\langle R\rangle_{norm}$) and from binary numbers ($\sin(\langle R_b\rangle_{norm}\pi/2)$).

3.2. Frequency Domain

In the FD, because the S-parameters are complex numbers measured, to apply the one-bit correlation in (2), the real part and the imaginary part need to be treated separately. We define

$$R_{\mathrm{ReRe}}(\partial f) \equiv \frac{1}{f_2-f_1}\int_{f_1}^{f_2} \mathrm{Re}[S_{21}(f)]\mathrm{Re}[S_{21}(f+\partial f)]df$$

$$R_{\mathrm{ReIm}}(\partial f) \equiv \frac{1}{f_2-f_1}\int_{f_1}^{f_2} \mathrm{Re}[S_{21}(f)]\mathrm{Im}[S_{21}(f+\partial f)]df$$

$$R_{\mathrm{ImRe}}(\partial f) \equiv \frac{1}{f_2-f_1}\int_{f_1}^{f_2} \mathrm{Im}[S_{21}(f)]\mathrm{Re}[S_{21}(f+\partial f)]df$$

$$R_{\mathrm{ImIm}}(\partial f) \equiv \frac{1}{f_2-f_1}\int_{f_1}^{f_2} \mathrm{Im}[S_{21}(f)]\mathrm{Im}[S_{21}(f+\partial f)]df \quad (8)$$

From (2) we have

$$\langle R\rangle(\partial f) = \langle R_{\mathrm{ReRe}}\rangle(\partial f) + \langle R_{\mathrm{ImIm}}\rangle(\partial f) + j[\langle R_{\mathrm{ImRe}}\rangle(\partial f) - \langle R_{\mathrm{ReIm}}\rangle(\partial f)] \quad (9)$$

From (6), we have

$$\langle R_{\mathrm{ReRe}}\rangle(\partial f) = \sigma_{\mathrm{Re}}^2 \sin\left[\frac{\pi}{2}\langle R_{b\mathrm{ReRe}}\rangle(\partial f)\right] \quad (10)$$

$$\langle R_{\mathrm{ImRe}}\rangle(\partial f) = \sigma_{\mathrm{Im}}\sigma_{\mathrm{Re}} \sin\left[\frac{\pi}{2}\langle R_{b\mathrm{ImRe}}\rangle(\partial f)\right] \quad (11)$$

where R_{b*} is the correlation obtained using one-bit technique, $\sigma_{\mathrm{Re}} = \sqrt{\langle \mathrm{Re}[S_{21}(f)]^2\rangle}$, and $\sigma_{\mathrm{Im}} = \sqrt{\langle \mathrm{Im}[S_{21}(f)]^2\rangle}$. Similar expressions can also be obtained for $\langle R_{\mathrm{ImIm}}\rangle(\partial f)$ and $\langle R_{\mathrm{ReIm}}\rangle(\partial f)$.

The measured S_{21} in the frequency range of 2.8 GHz ~ 3 GHz are used to obtain the FD autocorrelations, 360 stirrer positions are used. The correlations of $\langle R_{\mathrm{ReRe}}\rangle$, $\langle R_{\mathrm{ImRe}}\rangle$, $\langle R_{\mathrm{ImIm}}\rangle$ and $\langle R_{\mathrm{ReIm}}\rangle$ are calculated using the one-bit technique, the results are illustrated in Fig.4*a* and *b*. Not surprisingly, if the RC is well-stirred, we have $\langle R_{\mathrm{ReRe}}\rangle(\partial f) = \langle R_{\mathrm{ImIm}}\rangle(\partial f)$ and $\langle R_{\mathrm{ImRe}}\rangle(\partial f) = \langle R_{\mathrm{ReIm}}\rangle(-\partial f)$. The normalised values of the FD autocorrelations are given in Fig.4*c* which shows good agreement. We can also extract the coherence bandwidth and relate it to the TD Q factor in an RC [26, 28, 34]. From Fig. 4*c*, when the normalised correlation is $1/\sqrt{2}$, we have the average mode bandwidth $\partial f = 0.74$ MHz. The centre frequency $f = 2$ GHz can be used. Thus, the average Q factor in the frequency range of 1 GHz – 3 GHz can be evaluated as $Q = f/\partial f \approx 2703$ [26, 28].

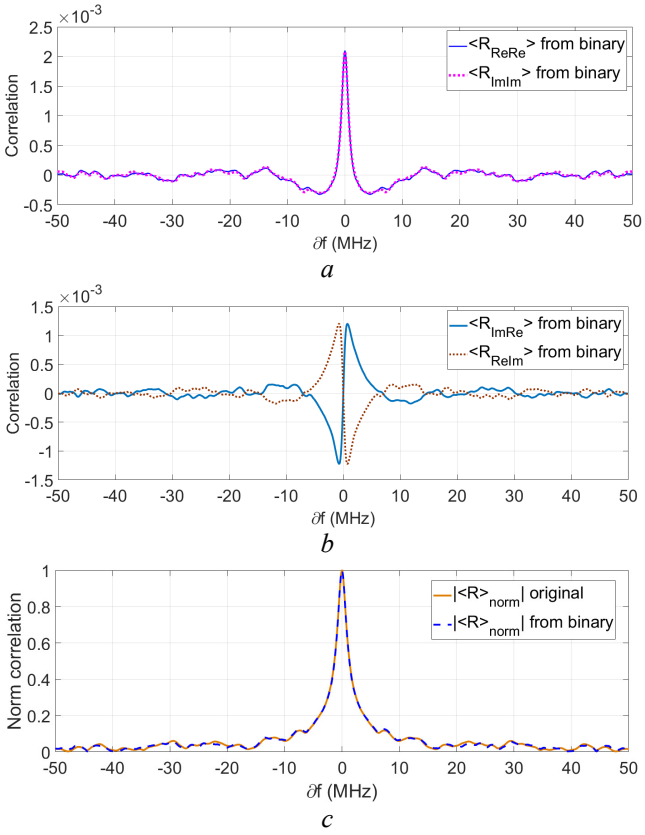

Fig.4. **(a)** FD correlations of $\langle R_{\mathrm{ReRe}}\rangle$ and $\langle R_{\mathrm{ImIm}}\rangle$ calculated using the one-bit technique, **(b)** correlations of $\langle R_{\mathrm{ImRe}}\rangle$ and $\langle R_{\mathrm{ReIm}}\rangle$ calculated using the one-bit technique, **(c)** the magnitude of the normalised autocorrelations calculated from float numbers and from binary numbers.

3.3. Space Domain

To verify the results in the SD, we measured S_{21} in the frequency range of 2.8 GHz ~ 3.0 GHz with 2001 sample points. 1800 stirrer positions were used with 0.2°/step.

In this case, the average operation $\langle\cdot\rangle$ is applied over different frequencies but not over different stirrer positions. By replacing f with θ in (8) - (11), the angular correlations of $\langle R_{\mathrm{ReRe}}\rangle$, $\langle R_{\mathrm{ImRe}}\rangle$, $\langle R_{\mathrm{ImIm}}\rangle$ and $\langle R_{\mathrm{ReIm}}\rangle$ are calculated using the one-bit technique (in Fig.5*a* and *b*). The normalised values of the angular autocorrelations are given in Fig.5*c*. As expected, they agree well with each other. The independent sample number can be extracted from the correlation angle for a given correlation threshold [28-30]. If a threshold of $1/e \approx 0.37$ is used, the correlation angle can be obtained as $\partial\theta = 3.8°$, thus in the measured frequency range, the number of independent samples the stirrer can provide for one full rotation is $360°/3.8° \approx 95$.

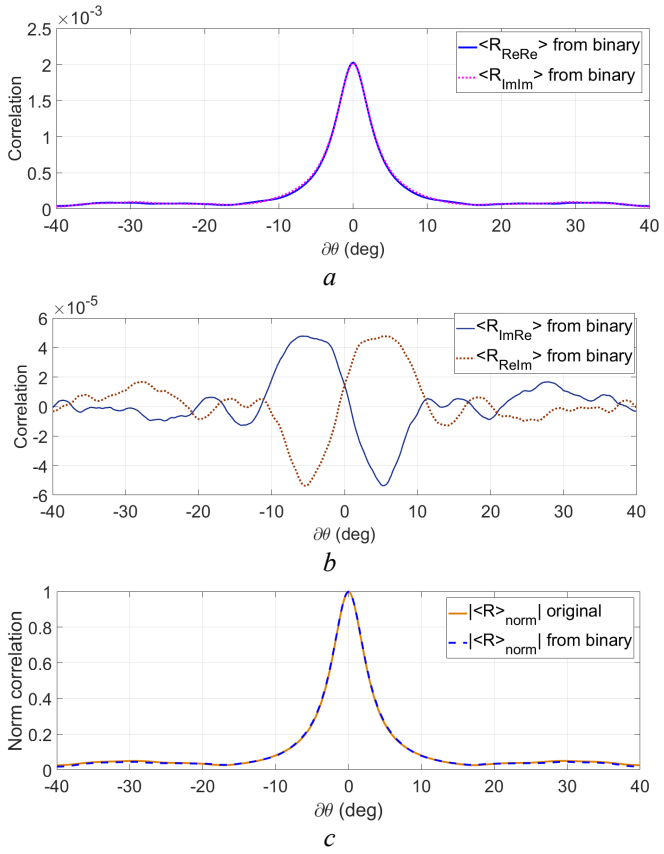

Fig. 5. **(a)** Angular correlations of $\langle R_{\mathrm{ReRe}} \rangle$ and $\langle R_{\mathrm{ImIm}} \rangle$ calculated using the one-bit technique, **(b)** correlations of $\langle R_{\mathrm{ImRe}} \rangle$ and $\langle R_{\mathrm{ReIm}} \rangle$ calculated using the one-bit technique, **(c)** the magnitude of the normalised autocorrelations calculated from float numbers and from binary numbers.

4. Conclusions

The one-bit correlation technique has been applied to the data processing measured in an RC. Correlations in the TD, FD and SD have been calculated by using the one-bit technique and compared with the original results. We have also generalised the one-bit technique to complex numbers which requires calculating the real part and imaginary part separately. As expected, the results show good agreement, and the one-bit correlation can be used in the correlation measurement in an RC.

If we check the calculation process using one-bit technique, it actually simplifies the multiplications to boolean operations and the float number integral to integer number counting. This reduces the computation complexity greatly, as logical operations and integer number counting are much faster than float number calculations for hardware. Based on this method, it is possible to accelerate the measurements in an RC using a programmable hardware (e.g. field-programmable gate array, FPGA) to realise a real time measurement system. This could be very useful for the testbed for the next generation (5G) OTA measurements and characterisations.

5. Acknowledgments

This work was supported in part by the National Natural Science Foundation of China (61701224 and 61601219) and Nature Science Foundation of Jiangsu Province (BK20160804).

6. References

[1] Hill, D. A.: 'Electromagnetic Fields in Cavities: Deterministic and Statistical Theories', Wiley-IEEE Press, 2009.

[2] Besnier, P., Démoulin, B.: 'Electromagnetic Reverberation Chambers', Wiley, 2013.

[3] Boyes, S. J., Huang, Y.: 'Reverberation Chambers, Theory and Applications to EMC and Antenna Measurements', Wiley, 2016.

[4] Xu, Q., Huang, Y.: 'Anechoic and Reverberation Chambers: Theory, Design and Measurements,' Wiley-IEEE, 2018.

[5] Chen, X., Kildal, P., Carlsson, J. and Yang, J.: 'MRC diversity and MIMO capacity evaluations of multi-port antennas using reverberation chamber and anechoic chamber,' IEEE Transactions on Antennas and Propagation, 2013, 61, (2), pp. 917-926.

[6] Chen, X., Kildal, Orlenius, P. S., C. and Carlsson, J.: 'Channel sounding of loaded reverberation chamber for over-the-air testing of wireless devices: coherence bandwidth versus average mode bandwidth and delay spread,' IEEE Antennas and Wireless Propagation Letters, 2009, 8, pp. 678-681.

[7] Chen, X., Kildal, P. S. and Carlsson, J.: 'Determination of maximum Doppler shift in reverberation chamber using level crossing rate,' Proceedings of the 5th European Conference on Antennas and Propagation (EUCAP), Rome, Italy, 2011, pp. 62-65.

[8] Skårbratt, A., Åsberg, J. and Orlenius, C.: 'Over-the-air performance testing of wireless terminals by data throughput measurements in reverberation chamber,' Proceedings of the 5th European Conference on Antennas and Propagation (EUCAP), Rome, 2011, pp. 615-619.

[9] Einarsson, B. Þ., Hussain, A. and Kildal, P. S.: 'Measurements of throughput in reverberation chamber using universal software radio peripheral,' The 8th European Conference on Antennas and Propagation (EuCAP 2014), The Hague, 2014, pp. 1105-1108.

[10] Kildal, P. S., Glazunov, A. A.: 'OTA testing of 3G-5G devices with MIMO: From anechoic chambers to reverberation chambers and … back again?,' IEEE International Symposium on Antennas and Propagation & USNC/URSI National Radio Science Meeting, San Diego, CA, 2017, pp. 1697-1698.

[11] Chen, X.: 'Experimental investigation and modeling of the throughput of a 2×2 closed-loop MIMO system in a reverberation chamber,' IEEE Transactions on Antennas and Propagation, 2014, 62, (9), pp. 4832-4835.

[12] Patané, C. L., Skårbratt, A. and Orlenius, C.: 'Basic and advanced MIMO OTA testing of wireless devices using reverberation chamber,' The 8th European Conference on Antennas and Propagation (EuCAP 2014), The Hague, 2014, pp. 3488-3492.

[13] Holloway, C. L., Hill, D. A., Ladbury, J. M., Wilson, P. F., Koepke, G. and Coder, J.: 'On the use of reverberation chambers to simulate a Rician radio environment for the testing of wireless devices,' IEEE Transactions on Antennas and Propagation, 2006, 54, (11), pp. 3167-3177.

[14] Chen, X., Einarsson, B. Þ. and Kildal, P. S.: 'Improved MIMO throughput with inverse power allocation—study using USRP measurement in reverberation chamber,' IEEE Antennas and Wireless Propagation Letters, 2014, 13, pp. 1494-1496.

[15] Hussain, A., Glazunov, A. A., Einarsson, B. Þ. and Kildal, P. S.: 'Antenna measurements in reverberation chamber using USRP,' IEEE Transactions on Antennas and Propagation, 2016, 64, (3), pp. 1152-1157.

[16] X. Chen and P. Kildal: "Verifying detection probabilities for MIMO system in reverberation chamber," *IEEE Conference on Antenna Measurements & Applications (CAMA)*, Antibes Juan-les-Pins, 2014, pp. 1-3.

[17] Hussain, A., Por Einarsson, B. and Kildal, P. S.: 'MIMO OTA testing of communication system using SDRs in reverberation chamber,' IEEE Antennas and Propagation Magazine, 2015, 57, (2), pp. 44-53.

[18] Shapiro, N. M., Campillo, M., Stehly, L. and Ritzwoller, M. H.: 'High-resolution surface-wave tomography from ambient seismic noise,' *Science*, 2015, 307, pp. 1615-1618.

[19] Hirata, S., Kurosawa, M. K. and Katagiri, T.: 'Cross-correlation by single-bit signal processing for ultrasonic distance measurement,' IEICE Transactions on Fundamentals of Electronics, Communications and Computer Sciences, 2008, E91-A, (4), pp. 1031-1037.

[20] Larose, E., Derode, A., Campillo, M. and Fink, M.: 'Imaging from one-bit correlations of wideband diffuse wave fields,' Journal of Applied Physics, 2014, 95, (12), pp. 8393-8399.

[21] Horner, J. L. and Bartelt, H. O.: 'Two-bit correlation,' Applied Optics, 1985, 24, (18), pp. 2889-2893.
[22] Davy, M., Rosny de J., Joly, J. –C., and Fink, M.: 'Focusing and amplification of electromagnetic waves by time reversal in an leaky reverberation chamber,' Comptes Rendus Pysique, 2010, 11, (1), pp. 37-43.
[23] Derode, A., Tourin, A. and Fink, M.: 'Untrasonic pulse compression with one-bit time reversal through multiple scattering,' Journal of Applied Physics, 1999, 85, (9), pp. 6343-6352.
[24] Hanasoge, S. M. and Branicki, M.: 'Interpreting cross-correlations of one-bit filtered seismic noise,' Geophysical Journal International, 2013, 195, pp. 1811-1830.
[25] Xu, Q., Huang, Y., Xing, L., Tian, Z., Stanley, M. and Yuan, S.: 'B-Scan in a reverberation chamber,' IEEE Transactions on Antennas and Propagation, 2016, 64, (5), pp. 1740-1750.
[26] Holloway, C. L., Shah, H. A., Pirkl, R. J., Remley, K. A., Hill, D. A. and Ladbury, J.: 'Early time behavior in reverberation chambers and its effect on the relationships between coherence bandwidth, chamber decay time, RMS delay spread, and the chamber buildup time,' IEEE Transactions on Electromagnetic Compatibility, 2012, 54, (4), pp. 714-725.
[27] Pirkl, R. J., Remley, K. A. and Patane, C. S. L.: 'Reverberation chamber measurement correlation,' IEEE Transactions on Electromagnetic Compatibility, 2012, 54, (3), pp. 533-545.
[28] Xu, Q., Xing, L., Zhao, Y., Tian, Z. and Huang, Y.: 'Wiener–Khinchin theorem in a reverberation chamber,' IEEE Transactions on Electromagnetic Compatibility, 2018, doi: 10.1109/TEMC.2018. 2863297.
[29] CTIA: 'Test Plane for Wireless Large-Form-Factor Device Over-the-Air Performance', Ed 1.1, 2017-07.
[30] IEC Standard: 'IEC 61000-4-21: Electromagnetic compatibility (EMC) – Part 4-21: Testing and measurement techniques – Reverberation chamber test methods', Ed 2.0, 2011-01.
[31] Tomoda, Y.: 'A simple method for calculating the correlation coefficients,' Journal of Physics of the Earth, 1956, 4, (2), pp. 67-70.
[32] Vleck, J. H. van, Middleton, D.: 'The spectrum of clipped noise,' Proceedings of the IEEE, 1966, 54, (1), pp. 2-19.
[33] Barari, M., Tavakoli, A., and Moini, R.: 'Analysis of Vivaldi antenna over a finite ground using a FDTD method,' IEEE International Symposium on Electromagnetic Compatibility, Istanbul, 2003, pp. 904-907.
[34] Delangre, O., Doncker, P. De, Lienard, M. and Degauque, P.: 'Delay spread and coherence bandwidth in reverberation chamber,' Electronics Letters, 2008, 44, (5), pp. 328-329.